International Journal of Microwave and Wireless Technologies

cambridge.org/mrf

Low profile dual band-stop super wideband printed monopole antenna with polarization diversity

Murli Manohar[1], Rakhesh Singh Kshetrimayum[2] and Anup Kumar Gogoi[2]

[1]Department of Electronics and Communications Engineering, IIIT Imphal 795 002, Manipur, India and
[2]Department of Electronics and Electrical Engineering, IIT Guwahati 781039, Assam, India

Research Paper

Cite this article: Manohar M, Kshetrimayum RS, Gogoi AK (2019). Low profile dual band-stop super wideband printed monopole antenna with polarization diversity. *International Journal of Microwave and Wireless Technologies* **11**, 694–702. https://doi.org/10.1017/S1759078719000175

Received: 11 May 2018
Revised: 29 January 2019
Accepted: 29 January 2019
First published online: 5 March 2019

Key words:
Dual band-notched antenna; polarization diversity; super wideband (SWB) antenna; tapered monopole antenna

Author for correspondence:
Murli Manohar
E-mail: murli@iiitmanipur.ac.in

Abstract

A low profile super-wideband polarization diversity printed monopole antenna with dual band-notched characteristics is presented the first time. The designed antenna comprises two arched shaped radiating elements with two triangular tapered microstrip feed lines (TTMFL) and two arched shaped partial ground planes, which covers an enormously wide impedance bandwidth (BW) from 1.2 to 25 GHz (ratio BW of 20.8:3) for reflection coefficient $|S_{11}| < -10$ dB. To ensure the high port isolation (better than -30 dB) between two feeding ports over the whole bands, two analogous antennas have been kept perpendicular to each other at a distance of 1 mm. In addition, the dual band-notched performance in wireless local area network (5–6 GHz) and X-band (7.2–8.5 GHz) is generated by employing a pair of open-circuited stubs (L-shaped stub and horizontal stub) to the TTMFL. Envelop correlation coefficient has been computed to study the polarization diversity performance. Finally, the proposed antenna was fabricated and tested successfully. Measured results indicate that the proposed antenna is an appropriate candidate for the polarization diversity applications. The proposed antenna has a compact size of $40 \times 70 \times 0.787$ mm^3, high isolation, and occupies a small space compared with the existing antennas.

Introduction

In contemporary wireless communication technology, polarization diversity is a key technique to diminish the multipath fading signals in the multipath environment and to enhance the capacity of the system in terms of the high data transmission [1]. Basically in polarization diversity schemes [2], two or more antennas are utilized at the transmitter and receiver for sending and receiving multiple signals simultaneously over a single channel to boost the quality and reliability of the data reception with good isolation. Therefore, in order to enhance the system performance and high data rate (up to 1000 Mbps) for short range (about 10 meters) wireless communications, polarization diversity is integrated with the ultrawideband (UWB) technology [3,4].

UWB [5] has become very popular among the recently developed technologies for wireless communications owing to its several fascinating features such as huge bandwidth (BW), low susceptibility to multipath fading, high data rate transmission, and large channel capacity. A number of UWB antennas with polarization diversity characteristics have been designed and reported in the literature [6–9]. To further enhance the channel capacity, a super wideband (ratio BW of more than 10:1) antenna with polarization diversity characteristics has been introduced in [10].

One significant problem to be noted for the UWB/super-wideband (SWB) antenna is that, it may cause electromagnetic interference with the existing narrow band wireless local-area network (WLAN) and X-band operating in 5.15–5.85 GHz and 7.25–8.395 GHz (for down link: 7.25–7.745 GHz and uplinks: 7.9–8.395 GHz) frequency bands. These narrow bands exist inside the UWB/SWB frequency range. To alleviate this interference issue, UWB/SWB antennas with band-notched characteristics have been proposed. A variety of UWB polarization-diversity antennas with band-notched functionality have been investigated in [11–16]. In ref [11] to realize the polarization diversity performance over the UWB, two pairs of differentially-fed monopoles were arranged perpendicularly and a band-notch characteristics at 5.5 GHz was achieved by etching the arched shaped slots. In ref [12] two half circled slot monopoles were placed in mirror configuration about the *y*-axis to achieve the polarization diversity and the two notches in the frequency band of 2--5 GHz and 7--11 GHz were achieved by employing the C-shaped slots on the radiating elements, while in ref [13] a pair of L-slits were etched on the ground plane to have the notched band characteristics at 5.5 GHz. In [14] two similar Koch fractal UWB antennas are placed at 90° to each other to deliver the polarization diversity operation and the band rejection phenomenon is realized by etching a C-shaped slot on the radiating

CAMBRIDGE UNIVERSITY PRESS

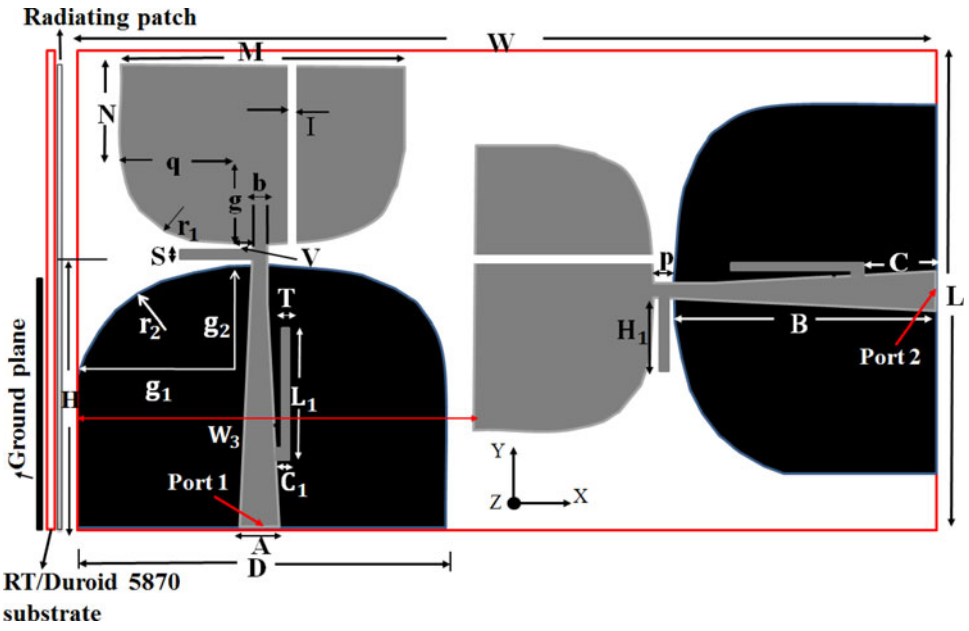

Fig. 1. Layout of the proposed antenna.

patch. A planar circular patch and a rectangular ground are used to attain UWB, and a triple band notched characteristic is obtained by etching two split ring slots and two arc on the radiating patch in ref [15]. In [16] an UWB circular disc patch antenna with semicircular arc slot loaded ground plane and a 50-Ω microstrip tapered feed line were adopted to enhance the impedance BW. Further, to generate the multiple stopbands a half mode substrate integrated waveguide cavity is employed below the feed line. However, the above-mentioned antennas have been designed to have notch within UWB region and occupies a large area, which may not be easily accommodated in the restricted space provided by some hand held electronic devices. In this paper authors have presented a compact SWB polarization diversity antenna with dual band-notched characteristics. Our new structure is smaller and offers better isolation than the other band-notched UWB diversity antennas [11–16] and the dual band-notched characteristics have been realized within the SWB region. Simulation results have been carried out with the finite element method (FEM)-based Ansoft high-frequency structure simulator (HFSS) software.The simulated and measured results show that the proposed antenna can deliver wide frequency BW (1.2–25 GHz) with high isolation in terms of S-parameters <– 30dB over the entire band of interest except for the two rejected bands in the frequency bands of 5–6 GHz (for WLAN) and 7.2–8.5 GHz (for X-band satellite communication system). In addition, measured radiation patterns and envelop correlation coefficient (0.025) results suggest that the proposed antenna has delivered reasonably well diversity performance.

Design and evolution of the proposed antenna

Antenna design

Figure 1 illustrates the configuration of the proposed SWB polarization diversity monopole antenna with dual band-notched functionality. The proposed antenna is fabricated on a low loss RT/Duroid 5870 substrate of thickness (h) 0.787 mm with a dielectric constant ε_r of 2.23, a loss tangent of 0.0012 and excited through two 3.5 mm SMA connectors. A 50-Ω triangular tapered microstrip feed lines (TTMFL) [17] is employed to feed the main arched shaped traveling wave radiating elements for broadband impedance matching. Because TTMFL involves continuous change impedance functions in a smooth fashion from the impedance of the one line to other line. Hence it is capable of supporting SWB radios without increasing the antenna dimensions. A closed form solution of the Riccati equation for triangularly tapered feed line is given by [17]

$$\Gamma(\theta) = \frac{1}{2} e^{-j\beta L} \ln\left(\frac{Z_L}{Z_0}\right) \left[\frac{\sin(\beta l_k/2)}{\beta l_k/2}\right]^2, \quad (1)$$

where Z_L is the load impedance, Z_0 is the characteristic impedance, $\Gamma(\theta)$ is the reflection coefficient, β is the phase constant and $l_k (l_k = B + P)$ is the triangular tapered feed line length. An arched shaped partial ground planes placed on the rear side of the substrate also play a vital role for further improving the impedance BW. The lower resonant frequency of a semi-circular printed monopole antenna is based on the equivalent cylindrical monopole, which can be estimated by mathematical formula [6]

$$f_L = \frac{v/4}{J + p + K/2\pi J}, \quad (2)$$

where J ($J = N + g$) is the length of the printed monopole antenna, v is the speed of light (m/s), K is the area of the semi-circle monopole radiating patch and p is the feeding gap distance of the printed monopole, respectively.

To realize a band-notched functionality in wireless local area network (5–6 GHz), an L-shaped open-circuited stub (LOCS) is employed with the TTMFL. The physical length (U_1) of LOCS is set to approximately $0.25\lambda_g$ (quarter wavelength transformer)

https://doi.org/10.1017/S1759078719000175 Published online by Cambridge University Press

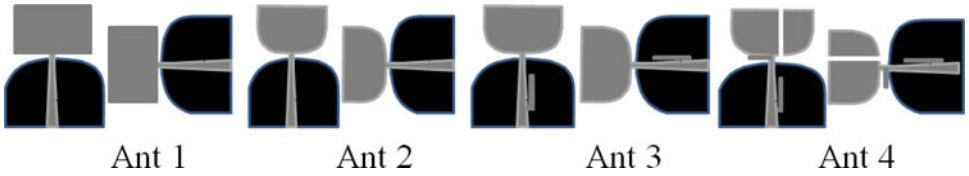

Fig. 2. Design evolution of the proposed antenna.

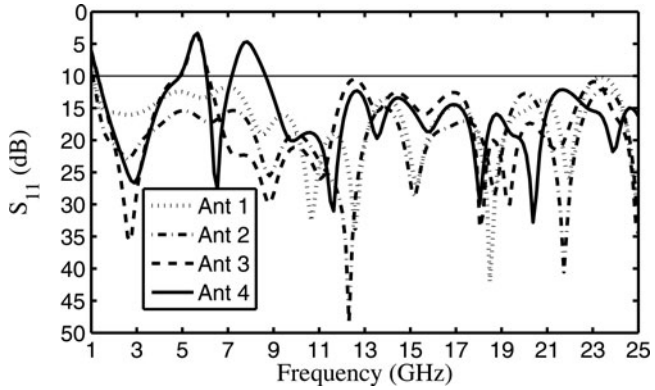

Fig. 3. Simulated return loss characteristics of antennas 1-4.

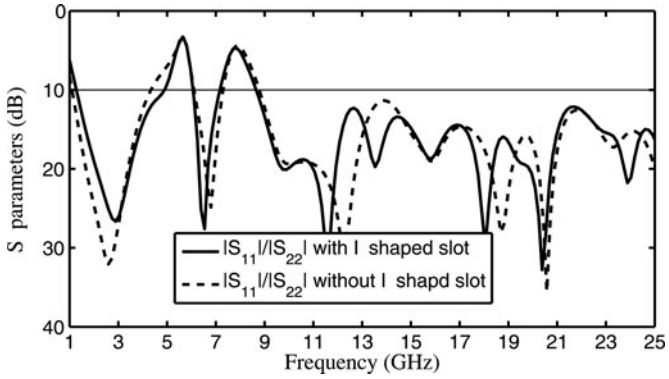

Fig. 4. Simulated S-parameters curve for with and without I-shaped slot.

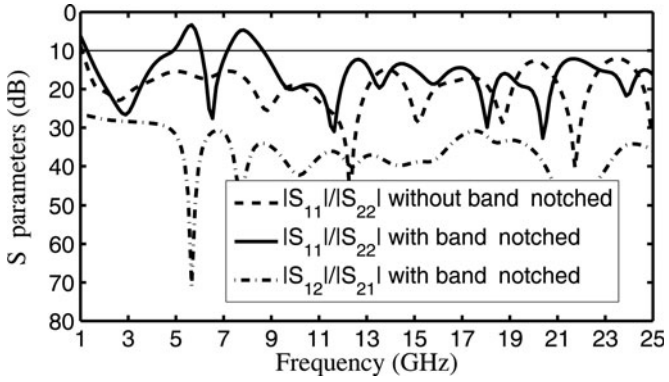

Fig. 5. Simulated S-parameters of the proposed antenna.

and can be expressed by numerical formula

$$U_1 = \frac{v}{4 f_{notch_1} \sqrt{\varepsilon_{eff}}}, \quad (3)$$

where ε_{eff} is the effective dielectric constant, v is the speed of light (m/s), f_{notch_1} is the center frequency of a corresponding central notched frequency at 5.5 GHz and $U_1 (U_1 = C_1 + L_1 - T)$ is the length of LOCS. The computed length of the LOCS from the equation (2) is found to be 8.6 mm. To obtain an another notched band characteristics at 7.2–8.5 GHz for X-band satellite system, a horizontal open-circuited stub (HOCS) is employed on the TTMFL. Similarly, calculated length $(U_2 = S + H_1)$ of the HOCS at central notched frequency (f_{notch_2}) 7.85 GHz from equation (4) is approximately equal to 5.7 mm and act as a half wavelength transformer $(0.5\lambda_g)$. The length of HOCS is chosen as:

$$U_2 = \frac{v}{2 f_{notch_2} \sqrt{\varepsilon_{eff}}}. \quad (4)$$

Evolution of the proposed antenna

Figure 2 depicts the involvement of various antenna structures to enhance the impedance BW and generate the desired dual band-notched functionality. Figure 3 represents the comparison results of the corresponding simulated reflection coefficients versus frequency graphs of Antennas 1-4. One can observe fromFig. 3 that an ordinary rectangular patch antenna (Antenna I) with arched shaped partial ground plane provides the wider impedance BW in the frequency band of 1.2–22.6 GHz. However, this antenna has poor impedance matching at a frequency of 23 GHz. In order to enlarge the impedance BW over the complete band, the lower-corner of the main radiator of Antenna II has been transformed into an arched shaped structure. The arched shaped patch (Antenna II) delivers an average return loss of around −18 dB in comparison to the Antenna I (around −13 dB) with rectangular patch. This is probably due to the advantageous capacitive load, which means that the antenna dominates the inductive reactance at the higher frequencies and produce almost purely resistive input impedance (Fig. 12). An LOCS is embedded with Antenna 3 to get a stopband function at the WLAN band. Lastly, to create an elimination at the X-band, a HOCS is employed on the TTMFL (i.e. Antenna IV). Further improving the characteristics of the first notched band (5–6 GHz), an I-shaped slot is inserted on the main patch as observed in Fig. 4. From Fig. 4 it is evident that without an I-shaped slot the notch frequency shifts 0.4 GHz lower in the first band-notch region and provides wider notch characteristics i.e. 4.6–6 GHz. This wide notched-band needlessly blocks usable frequencies from 4.6 to 5 GHz.

Two feeding ports (port 1 and port 2) are employed to excite the *X* (horizontal) and *Y* (vertical) polarization, respectively. Two identical radiating elements are placed orthogonal with each other, in order to achieve the high isolation between two feeding

https://doi.org/10.1017/S1759078719000175 Published online by Cambridge University Press

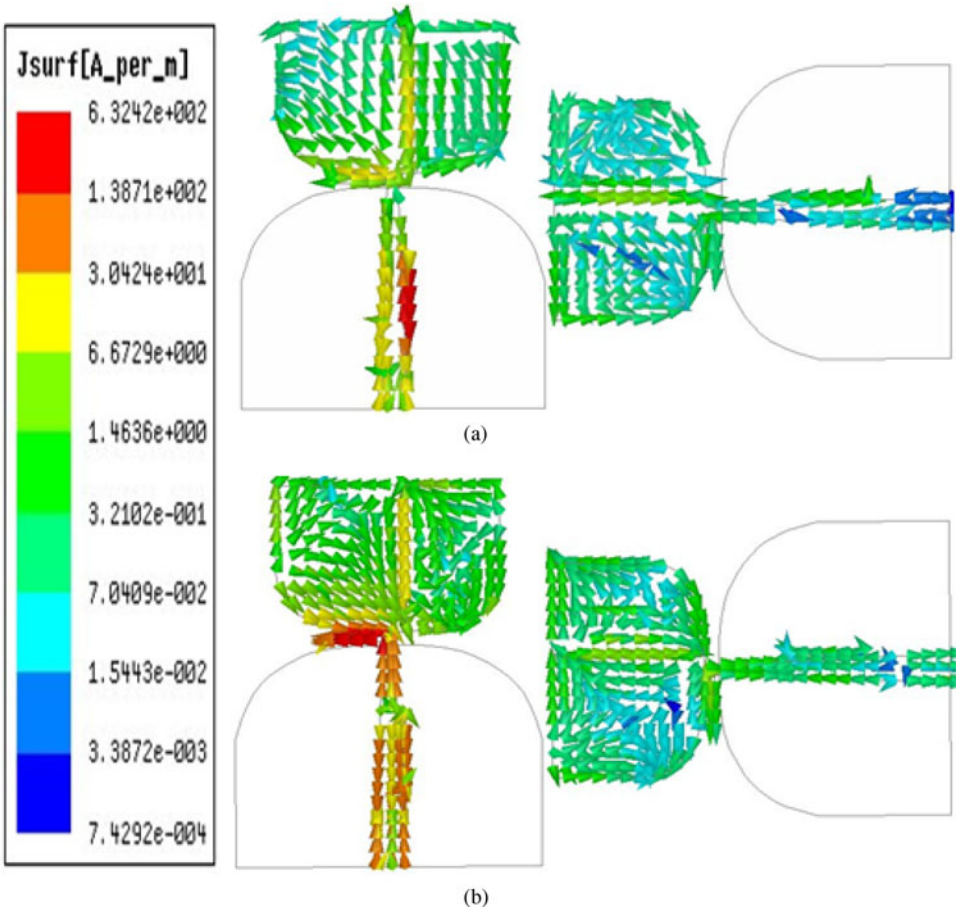

Fig. 6. Simulated surface current distribution of the proposed antenna at (a) 5.5 GHz (b) 7.85 GHz when port 1 is excited.

ports (port 1 and port 2) over the SWB region. Our proposed structure provides high isolation without any additional isolation elements [18], which makes the design and fabrication of the antenna a bit simple. To validate the aforesaid points such as extremely large BW, dual band-notched functionality and high isolation, the simulated S-parameters have been depicted in Fig. 5. FromFig. 5 it is observed that the average isolation ($|S_{12}|/|S_{21}|$) between the two ports is <−30 dB across the frequency band of 1.2–25 GHz except for two rejected bands, which fulfills the essence of polarization diversity antennas. In addition, the simulated $|S_{11}|/|S_{22}|$ with band-notched shows that the antenna starts operating from 1.2 to 25 GHz, except for the two rejected bands (denoted as $|S_{11}|/|S_{22}|$ with band-notched) at 5–6 GHz and 7.25–8.5 GHz, respectively. The optimal dimensions (derived using Ansoft HFSS version 14) of the proposed antennas are as follows: $L = 40$ mm, $W = 70$ mm, $M = 22$ mm, $N = 8$ mm, $I = 0.3$ mm, $V = 1$ mm, $p = 1.4$ mm, $B = 22.6$ mm, $W_3 = 31$ mm, $g = 7$ mm, $H = 23$ mm, $L_1 = 8$ mm, $T = 0.3$ mm, $C_1 = 0.3$ mm, $g_1 = 14.5$ mm, $g_2 = 9.6$ mm, $b = 1$ mm, $H_1 = 5.5$ mm, $q = 9.5$ mm, $r_1 = 8.32$ mm, $r_2 = 12.77$ mm, $C = 8.6$ mm, $A = 3$ mm, $D = 30$ mm, and $S = 0.5$ mm.

Results and discussions

Current distribution

In order to observe the physical behavior of the proposed antenna at two notched bands 5.5 and 7.85 GHz, the simulated surface current distribution plot is shown in Fig. 6 when port 1 is excited and port 2 is terminated with a 50-Ω load.

Since both ports (port 1 and port 2) are symmetrical, therefore current distribution is shown only for port 1. As can be seen, that the currents are mainly concentrated (indicated by red color) on LOCS and HOCS at the two resonant frequencies 5.5 and 7.85 GHz respectively, which shows that the antenna offers high suppression of radiation characteristics at the notched frequencies. In other words, most of the energy is reflected back at the notched frequencies, owing to the presence of LOCS and HOCS, while at the other frequencies, the signal is transferred successfully to the radiating element.

Parametric study

To obtain an intensive insight of how the proposed antenna's dimensions effect the overall antenna performance, a parametric analysis has been carried out. Figure 7 displays the simulated return loss ($|S_{11}|/|S_{22}|$) of the proposed antenna for different N. From Figure 7 it can be seen that by decreasing N from 8 to 6 mm, the percentage BW of the antenna significantly reduces from 90.8 to 89.3. Therefore, the optimized value of N=8 was selected. Figure 8 plots the simulated S-parameters for different W_3. It is observed that decreasing the value of W_3 from 31 to 29 mm leads to worsening the performance of average isolation between port 1 and port 2 within the UWB region as well as high-frequency region. With the increase of W_3 from 31 to 32 mm, a high isolation

https://doi.org/10.1017/S1759078719000175 Published online by Cambridge University Press

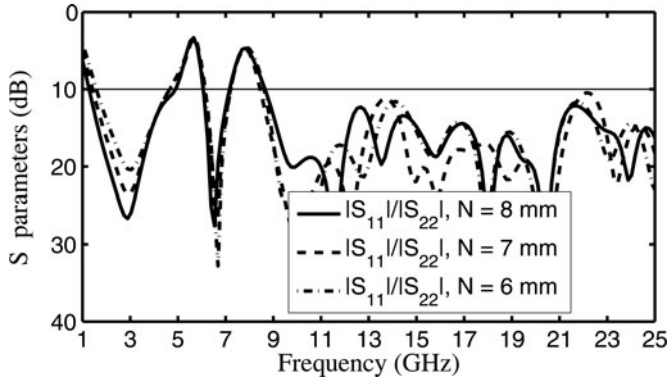

Fig. 7. Simulated S-parameters of the proposed antenna for different N.

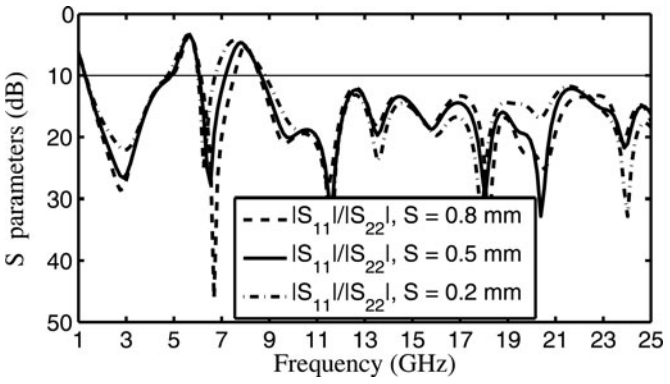

Fig. 9. Simulated S-parameters of the proposed antenna for different S.

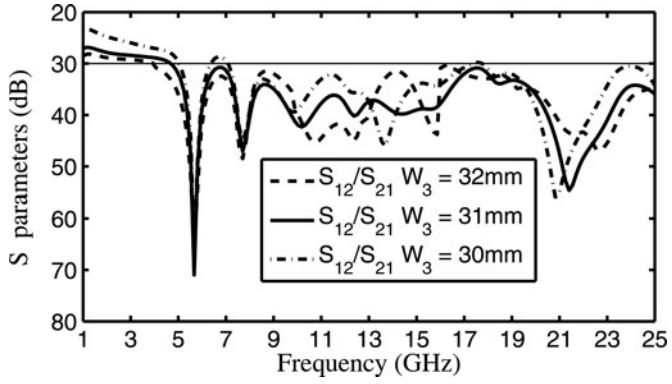

Fig. 8. Simulated S-parameters of the proposed antenna for different W_3.

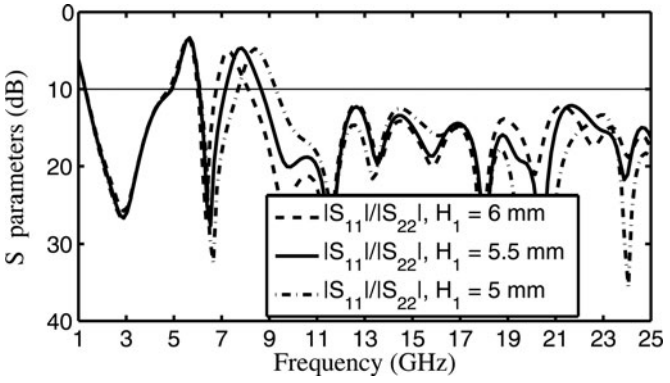

Fig. 10. Simulated S-parameters of the proposed antenna for different H_1.

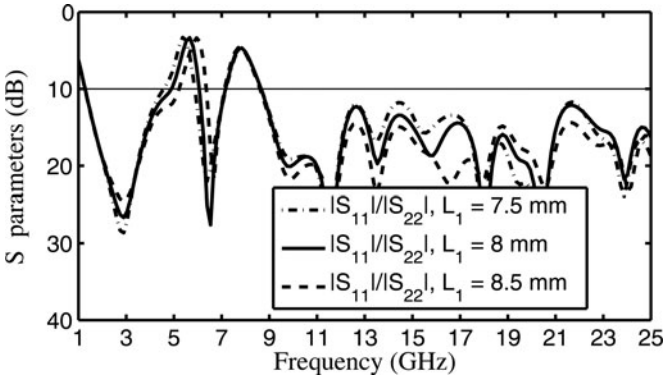

Fig. 11. Simulated S-parameters of the proposed antenna for different L_1.

($|S_{21}|/|S_{12}| \geq 30$ dB) can be obtained up to 13 GHz, whereas the performance of an average isolation reduces beyond 13 GHz. Therefore, favorable value of W_3 is set to be 31 mm to achieve the port isolation better than -32 dB for the entire band. Figures 9, 10, and 11 shows how the key parameters S, H_1, and L_1, flexibly controls the two notched bands. From Figs 9 and 10 it can be observed that by increasing the values of S and H_1 from (0.2, 5 mm) to (0.8, 6 mm), the first notched band remains insensitive, however second notched band moves towards left side from 8.95 and 8.5 GHz to 6.85 and 7.2 GHz, respectively. From these outcomes, we can conclude that the notched frequency can be easily controlled by varying the value of H_1. Moreover, as shown in Fig. 11 increasing the value of L_1 from 7.5 to 8.5 mm with other parameters fixed results in a first notched band shifted from 5.3 to 6 GHz, whereas the second notched band remains insensitive. Therefore, the impedance BW of notch frequency is controllable by adjusting the values of H_1 and L_1.

Equivalent circuit

Figure 12 represents the simulated input impedance of the proposed antenna. As shown in Fig. 12, by introducing a pair of open-circuited stubs two anti resonances are introduced at 5.5 and 7.85 GHz. The real part of the impedance of antenna at the frequency where the reactance is zero is called the resonant frequency. At notched frequency 5.5 GHz, the real part of the input impedance is maximum (150-Ω), when its imaginary component graph is zero crossing (behaves as a parallel LC resonator). However at frequency 7.85 GHz, the real component is minimum (approximately close to zero) and imaginary component graph behaves as a series LC resonator. On the other hand in the pass-band frequencies the reflection coefficient $|S_{11}| < -10$ dB can be achieved owing to multiple resonances excited by the proposed SWB antenna and each resonance can be considered as a parallel RLC circuit. The series and parallel LC resonators shown in Fig. 13 denote the contribution of the two notches, whereas several parallel RLC resonators are responsible for the wide impedance BW. The equivalent circuit input impedance can be represented as [19]

$$Z_{in} = Z_p + Z_s + \sum_{n=1}^{\infty} \frac{j\omega.R_k.L_k}{R_k.(1-\omega^2.L_k.C_k) + j\omega.L_k}, \qquad (5)$$

https://doi.org/10.1017/S1759078719000175 Published online by Cambridge University Press

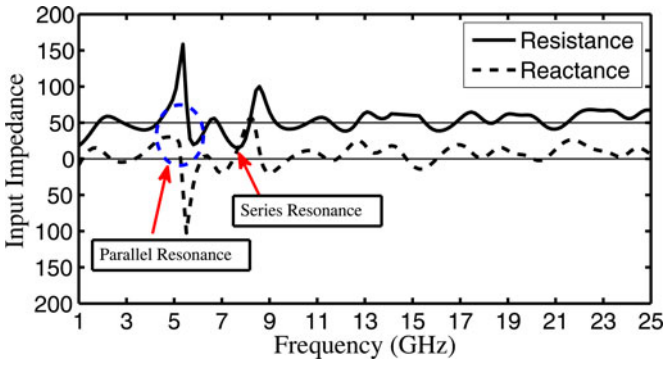

Fig. 12. Input impedance of the proposed antenna.

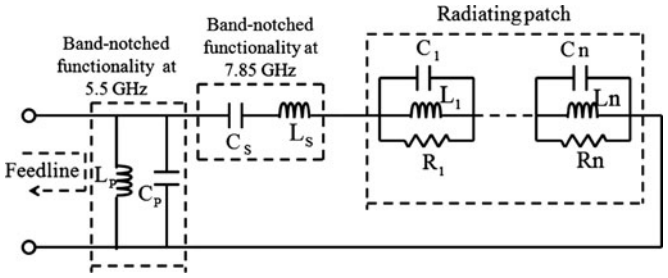

Fig. 13. Equivalent circuit model of the proposed antenna.

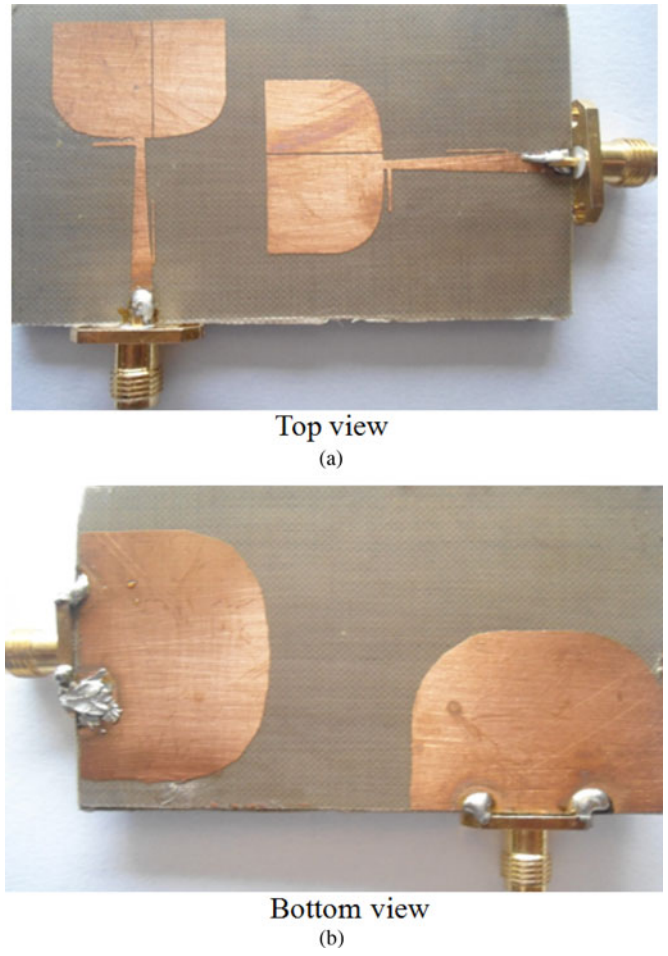

Fig. 14. Photograph of the fabricated antenna.

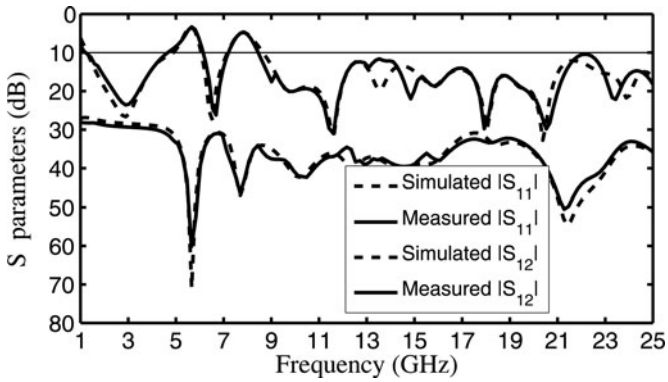

Fig. 15. Simulated and measured S-parameters of the proposed antenna.

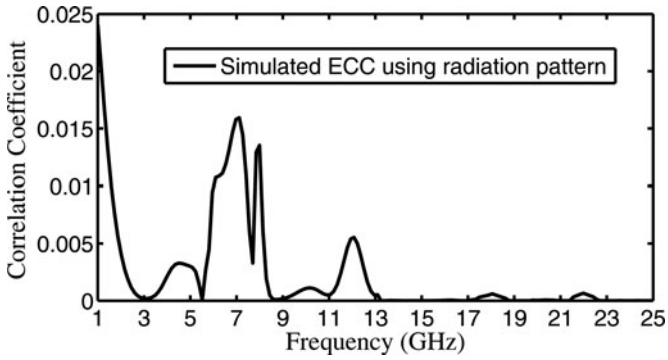

Fig. 16. ECC of the proposed antenna.

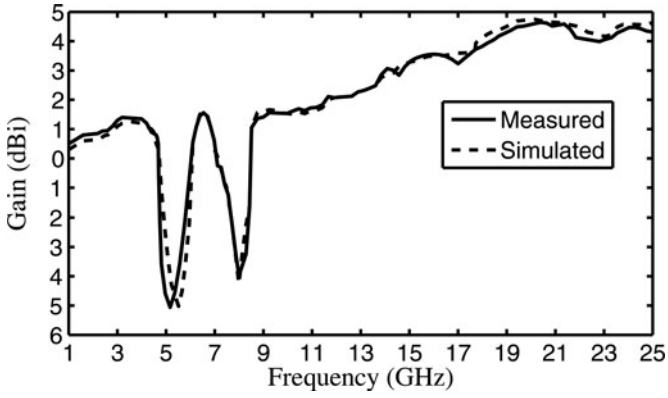

Fig. 17. Simulated and measured gain of the proposed antenna.

Table 1. Comparison of the size, BW, and isolation of the proposed antennas with other antennas

Ref. No.	Dimensions ($W \times L \times h$)	Ratio BW and Isolation (dB)
Ref. [11]	$64 \times 64 \times 0.8$ mm^3	3.6:6 and − 50
Ref. [12]	$68 \times 40 \times 1.6$ mm^3	3.9:2 and − 22
Ref. [13]	$38.5 \times 38.5 \times 1.6$ mm^3	3.8:3 and − 15
Ref. [14]	$45 \times 45 \times 1.6$ mm^3	5.0:3 and − 25
Proposed antenna	$70 \times 40 \times 0.787$ mm^3	15.6:2 and − 30

https://doi.org/10.1017/S1759078719000175 Published online by Cambridge University Press

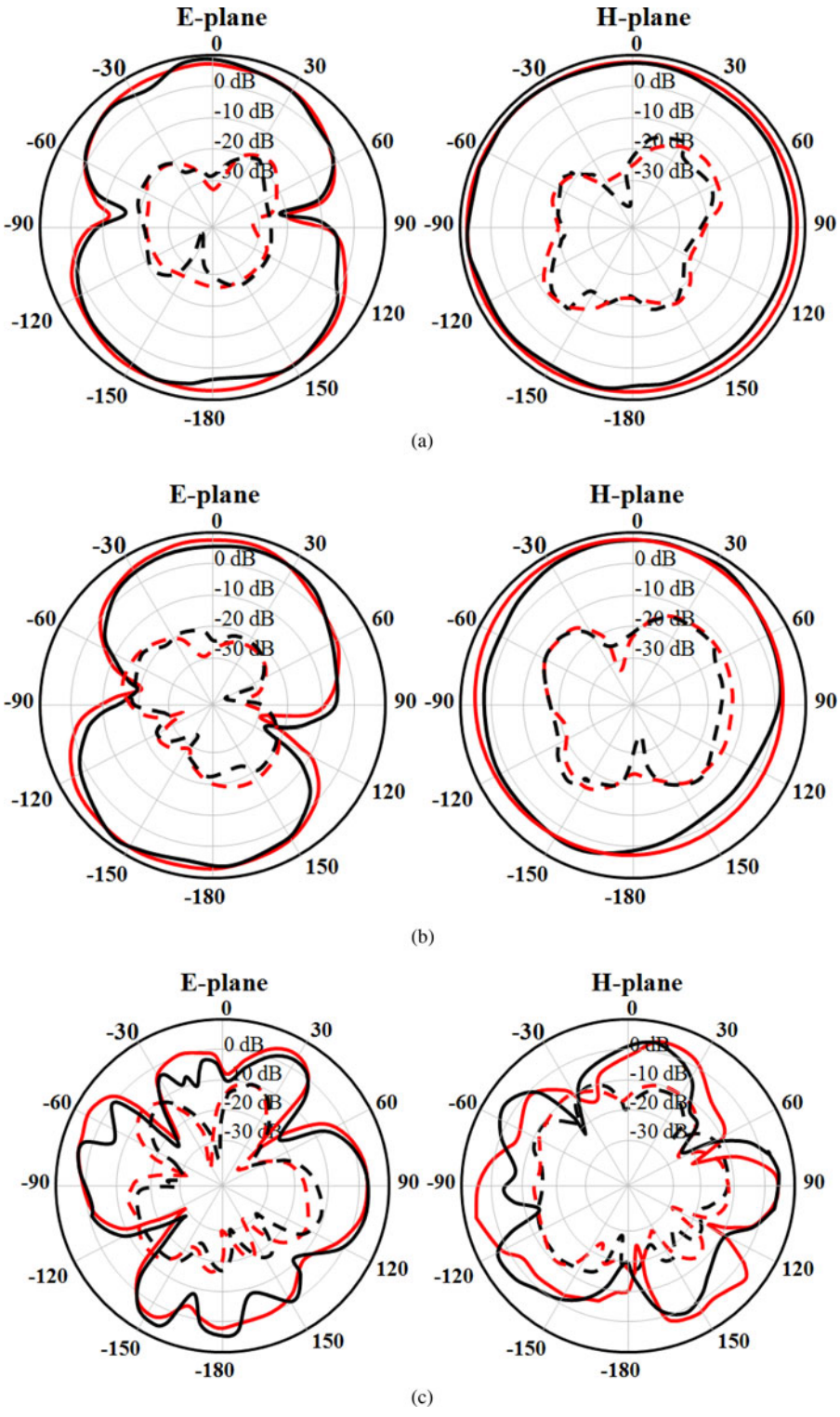

Fig. 18. Simulated (red) and measured (black) 2D far-field radiation patterns of the proposed antenna for different frequencies (a) 3.1 GHz (b) 10.6 GHz, and (c) 20 GHz (solid line is co-polarization and dashed line is cross-polarization).

where

$$Z_p = \frac{j\omega L_p}{\left(1 - \omega^2 L_p C_p\right)}, \tag{6}$$

$$Z_s = \frac{j(\omega^2 L_s C_s - 1)}{\omega C_s}. \tag{7}$$

Experimental results

The proposed antenna's layout is presented in Fig. 14. The measured impedance BW of the proposed antenna is carried out by a Rodhe and Schwarz ZVA24 vector network analyzer. Figure 15 shows a reasonably good agreement between the measured results and the simulated one across the specified frequency range from 1.2 -to 25 GHz with dual notched band of 5–6 GHz and 7.2–8.5 GHz, respectively.

https://doi.org/10.1017/S1759078719000175 Published online by Cambridge University Press

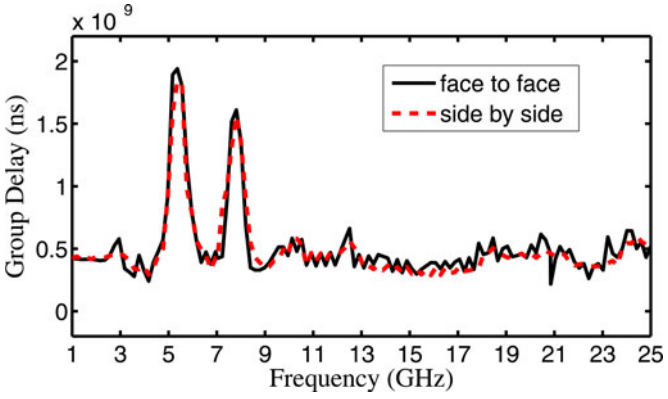

Fig. 19. Group delay of the proposed antenna.

Diversity performance

The diversity performance of the proposed antenna can be evaluated by computing the envelope correlation coefficient (ECC) from the radiation pattern as described in [20]. The purpose of calculating the value of ECC is to estimate how much the communication channels of the proposed antenna are isolated to each other. For reasonably well diversity performance of an antenna pair, the value of ECC should be <0.5 and can be estimated using far-field radiation pattern-based formula stated below [20]

$$\rho = \frac{\left|\iint_{4\pi} \vec{E}^{1}(\theta,\phi) \bullet \left(\vec{E}^{2}(\theta,\phi)\right)^{*} d\Omega\right|}{\sqrt{\iint_{4\pi}\left|\vec{E}^{1}(\theta,\phi)\right|^{2} d\Omega \iint_{4\pi}\left|\vec{E}^{2}(\theta,\phi)\right|^{2} d\Omega}}, \quad (8)$$

where $\vec{E}^{i}(\theta,\phi) = E^{i}_{\theta}\hat{\theta} + E^{i}_{\phi}\hat{\phi}$ is the radiation field of the antenna system when i^{th} port is excited, and E_θ and E_ϕ are the components in the direction of $\hat{\theta}$ and $\hat{\phi}$, respectively. The simulated result of ECC is plotted in Fig. 16. It is observed that over the entire frequency band (including two notches) correlation coefficient is below 0.025 which satisfies a good diversity performance.

Radiation pattern and gain

A peak gain is measured by gain transfer technique [21] where a typical broadband horn antenna was utilized to radiate the total power to the proposed antenna. Figure 17 illustrates the simulated and measured outcomes of the proposed antenna. The measured antenna gain shown in Fig. 17 is reduced to − 5.2 and − 4.1 dBi in the two stopbands from 5 to 6 GHz (WLAN) and 7–8 GHz (X-band satellite communication), respectively. However, the average gain of the proposed antenna beyond the notched bands is about 4.8 dBi. Table 1 depicts the dimension, ratio BW and isolation of the proposed antenna with existing antennas. The simulated and measured 2D far-field radiation patterns for port 1 of the proposed antenna in the *E*-plane (*xy*-plane) and *H*-plane (*xz*-plane) at 3.1, 10.6, and 20 GHz are shown in Fig. 18. Since both the ports are identical, therefore in the Fig. 18 port 1 is excited, while port 2 is terminated by a 50-Ω. It is evident that the *H*-plane (*xz*-plane port 1 and *xy*-plane port 2) patterns are nearly omnidirectional and relatively stable (variation is <− 10 dB) at frequencies 3.1 and 10.6 GHz. The *E*-plane (*xy*-plane port 1 and *xz*-plane port 2) radiation patterns at 3.1 and 10.6 GHz are directed maximum towards − *Y*-direction, showing the dipole-like (figure- of-eight) radiation patterns. The cross-polarization levels are approximately − 20 dB in the *E*- and *H*-planes at 3.1 and 10.6 GHz. However, in the *E*- and *H*-planes, it can be observed that at 20 GHz the cross-polarization level rises. Moreover, since the port 1 (vertical polarization) and port 2 (horizontal polarization) are oriented by 90° with each other, therefore the proposed antenna generates a considerably well orthogonal polarization performance.

Time domain characteristics

Group delay [22] is one of the most important parameter in communication system, which shows the degree of distortion of SWB pulse. Group delay is the measure of a signal transition time through a device. It is measured by keeping two identical antennas at a distance of 60 cm in the far field region in face-to-face and side-by-side orientations. The measured group delays for the face-to-face and side-by-side antenna results over the frequency from 1 to 25 GHz is presented in Fig. 19. From the graph, we can observe that the group delay is increased in the notch band, however variation of group delay is <0.7 ns outside the notched-band.

Conclusion

A compact SWB polarization diversity printed monopole antenna with dual band-notched functionality has been investigated in this communication. The proposed antenna provides an extremely large impedance BW in the frequency band of 1.2–25 GHz (ratio BW of 20.8:3) with dual band-notched characteristics covering the WLAN band and X-band satellite communication.To achieve the isolation better than − 30 dB (low mutual coupling) in the SWB band, two identical monopole antennas have been placed orthogonal to each other at a distance of 1 mm. Moreover, The proposed antenna possesses minimum ECC of 0.025 over the SWB frequency range, authenticating it a suitable candidate for polarization diversity applications. Due to large BW this antenna may also be used for spectrum sensing in cognitive radio [23].

References

1. **Foschini G and Gans MJ** (1998) On limits of wireless communications in a fading environment when using multiple antennas. *Wireless Personal Communications* **6**, 311–335.
2. **Vaughan RG and Andersen JB** (1987) Antenna diversity in mobile communications. *IEEE Transactions on Vehicular Technology* **36**, 147–172.
3. **Wang A, Zhenghe F and Luk KM** (2009) Pattern and polarization diversity antenna with high isolation for portable wireless devices. *IEEE Antennas Wireless Propagation Letters* **8**, 209–211.
4. **Chen ZN and See TSP** (2009) Diversity and its applications in ultrawideband antennas, Proccedings of IEEE International Workshop Antenna Technology, Santa Monica, CA, USA, March 2009pp. 1–4.
5. **Chen FCC** (2002) First report and order in the matter of revision of part 15 of the commission's rules regarding Ultra-Wideband Transmission Systems, ET-Docket, April 22,pp. 98–153.
6. **Koohestani M, Moreira AA and Skrivervik AK** (2014) A novel compact CPW-fed polarization diversity ultrawideband antenna. *IEEE Antennas Wireless Propagation Letters* **13**, 563–566.
7. **Wang L, Xu L, Chen X, Yang R, Han L and Zhang W** (2014) A compact ultrawideband diversity antenna with high isolation. *IEEE Antennas Wireless Propagation Letters* **13**, 35–38.

https://doi.org/10.1017/S1759078719000175 Published online by Cambridge University Press

8. **Adamiuk G, Zwick T and Wiesbeck W** (2010) Compact dual-polarized UWB-antenna embedded in a dielectric. *IEEE Transactions on Antennas and Propagation* **52**, 279–286.
9. **Chacko BP, Augustin G and Denidni TA** (2013) Uniplanar slot antenna for ultrawideband polarization-diversity applications. *IEEE Antennas Wireless Propagation Letters* **12**, 88–91.
10. **Liu J, Esselle KP, Hay SG, Sun Z and Zhong S** (2013) A compact super-wideband antenna pair with polarization diversity. *IEEE Antennas Wireless Propagation Letters* **12**, 1472–1475.
11. **Huang H, Liu Y, Zhang S and Gong S** (2014) Uniplanar differentially-driven ultrawideband polarization diversity antenna with band-notched characteristics. *IEEE Antennas Wireless Propagation Letters* **14**, 563–566.
12. **Ramkiran DS, Madhav BTP, Reddy KN, Shabbeer S, Jain P and Sowmya S** (2016) Coplanar wave guide fed dual band notched MIMO antenna. *International Journal of Electrical and computer Engineering* **6**, 1732–1741.
13. **Kang L, Li H, Wang X and Shi X** (2015) Compact offset microstrip-fed MIMO antenna for band-notched UWB application. *IEEE Antennas Wireless Propagation Letters* **14**, 1754–1757.
14. **Tripathi S, Mohan A and Yadav S** (2015) A compact koch fractal UWB MIMO antenna with WLAN band-rejection. *IEEE Antennas Wireless Propagation Letters* **14**, 1565–1568.
15. **Zhang Y, Hong W, Yu C, Kuai ZQ, Don YD and Zhou JY** (2008) Planar ultrawideband ntennas with multiple notched bands based on etched slots on the patch and/or split ring resonators on the feed line. *IEEE Transactions on Antennas and Propagation* **56**, 3063–3068.
16. **Dong YD, Hong W, Kuai ZQ, Yu C, Zhang Y, Zhou JY and Chen JX** (2008) Development of ultrawideband antenna with multiple band-notched characteristics using half mode substrate integrated waveguide cavity technology. *IEEE Transactions on Antennas and Propagation* **56**, 2894–2902.
17. **Mathur SP and Sinha AK** (1988) Design of microstrip exponentially tapered lines to match helical antennas to standard coaxial transmission lines. *IEE Proceedings, Microwaves, Antennas and Propagation* **135**, 272–274.
18. **Kumar R and Surushe G** (2016) Design of microstrip-fed printed UWB diversity antenna with tee crossed shaped structure. *International Journal of Engineering Science and Technology* **19** 946–955.
19. **Moradikordalivand A, Rahman TA, Ebrahimi S and Hakimi S** (2014) An equivalent circuit model for broadband modified rectangular microstrip-fed monopole antenna. *Wireless Personal Communications* **77** 1363–1375.
20. **Jaafreh SA, Huang Y and Xing L** (2016) Low profile and wideband planar inverted-F antenna with polarisation and pattern diversities. *IET Microwaves, Antennas and Propagation* **10** 152–161.
21. **Stutzman WL and Thiele GA** (2012) Antenna theory and design, John Wiley and Sons, Technology and Engineering.
22. **Lee JN, Kwon HK, Kang BS and Lee KC** (2013) Design of an ultra-wideband antenna using a ring resonator with a notch function. *Electronics and Telecommunications Research Institute (ETRI)* **35**, 1075–1083.
23. **Grayaver E** (2013) *Implementing Software Defined Radio*, New York: Springer.

Murli Manohar received the Ph.D. degree in Electronics and Electrical Engineering from the Indian Institute of Technology Guwahati, India in April 2015. He is presently working as an assistant professor in the Dept. of Electronics and Communication Engineering, Indian Inst. of Information Technology Manipur, India. His main research area is in antenna and RF engineering with focus on SWB printed monopole antenna.

Rakhesh Singh Kshetrimayum received the Ph.D. degree from the School of Electrical and Electronic Engineering (EEE), Nanyang Technological University (NTU) Singapore in 2005. Since 2005, he has been with the Dept. of EEE, IIT Guwahati as an Associate Professor (2010-), Assistant Professor (2006–10) and Senior Lecturer (2005–2006). He worked as a Postdoctoral Scholar at the Dept. of EE, Pennsylvania State University (PSU), USA (2005), Research Associate Provisional at the Dept. of Electrical Communication Engineering (ECE), Indian Inst. of Science (IISc) Bangalore (2004–2005), Teaching Assistant at the School of EEE, NTU Singapore (2002–2003) and Trainee Software Engineer at Mphasis, India (2000–2001). Dr. Kshetrimayum is the recipient of SEFOGG Young Engineer Award (2011), Dept. of Science & Technology India (SERC) Fast Track Scheme for Young Scientists (2007–2010) and NTU Research Scholarship from 2001–2004. His current areas of research interests are in printed antennas and circuits, UWB communications and MIMO wireless communications. He has been involved in organizing several IEEE international conferences as Technical program co-chair, Publication chair, Program chair, Session chair and Technical program committee. He is the Editor-in- Chief of Inderscience journal International Journal of Ultra Wideband Communications and Systems. He is a Life Fellow of the Institution of Electronics and Telecommunication Engineers (IETE), India, Optical Society of India (OSI) and Antenna Test & Measurement Society (ATMS), India; a senior member of the International Association of Computer Science and Information Technology (IACSIT), Singapore, and the Inst. of Electrical and Electronics Engineers (IEEE), USA; a member of the Applied Computational Electromagnetics Society (ACES), USA and the European Microwave Association (EuMA), Belgium.

Anup Kumar Gogoi is a Professor of Electronics and Electrical Engineering and Dean of Outreach Education Programme at the Indian Institute of Technology Guwahati. He received his Ph.D. degree from the Dept. of Electrical Engineering, Indian Inst. of Technology Kanpur. His areas of research interests are in electromagnetics, microwave engineering, RF circuits, and systems design.

https://doi.org/10.1017/S1759078719000175 Published online by Cambridge University Press